

THE HALO MASS FUNCTION CONDITIONED ON DENSITY FROM THE MILLENNIUM SIMULATION: INSIGHTS INTO MISSING BARYONS AND GALAXY MASS FUNCTIONS

A. FALTENBACHER^{1,2,3}, A. FINOGENOV^{4,5} & N. DRORY⁴

Draft version August 9, 2018

ABSTRACT

The baryon content of high-density regions in the universe is relevant to two critical unanswered questions: the workings of nurture effects on galaxies and the whereabouts of the missing baryons. In this paper, we analyze the distribution of dark matter and semianalytical galaxies in the Millennium Simulation to investigate these problems. Applying the same density field reconstruction schemes as used for the overall matter distribution to the matter locked in halos we study the mass contribution of halos to the total mass budget at various background field densities, i.e., the conditional halo mass function. In this context, we present a simple fitting formula for the cumulative mass function accurate to $\lesssim 5\%$ for halo masses between 10^{10} and $10^{15} h^{-1} M_{\odot}$. We find that in dense environments the halo mass function becomes top heavy and present corresponding fitting formulae for different redshifts. We demonstrate that the major fraction of matter in high-density fields is associated with galaxy groups. Since current X-ray surveys are able to nearly recover the universal baryon fraction within groups, our results indicate that the major part of the so-far undetected warm-hot intergalactic medium resides in low-density regions. Similarly, we show that the differences in galaxy mass functions with environment seen in observed and simulated data stem predominantly from differences in the mass distribution of halos. In particular, the hump in the galaxy mass function is associated with the central group galaxies, and the bimodality observed in the galaxy mass function is therefore interpreted as that of central galaxies versus satellites.

Subject headings: cosmology: large-scale structure of universe — galaxies: groups: general — method: numerical

1. INTRODUCTION

The environmental dependence of galaxy properties, such as broadband color, star formation, and stellar mass, is a well-known effect in the local universe (Dressler 1980). In this context environment means an estimate of the smoothed density field at a given location. Of particular interest for the present study is the dependence of the galaxy stellar mass function (GMF) on environment. Recent comprehensive galaxy redshift surveys have led to intensive studies in this field. For instance, Mo et al. (2004) model the dependence of the luminosity function on the large-scale environment based on mock catalogs for the the two-degree Field Galaxy Redshift Survey (2dFGRS; Colless et al. 2001) and Baldry et al. (2006) investigate the GMF as a function of environment in the nearby universe based on the Sloan Digital Sky Survey (SDSS; York et al. 2000). To uncover evolutionary effects, surveys spanning a larger redshift range have been used: the study by Bundy et al. (2006) is based on the DEEP2 Galaxy Redshift Survey ($0.4 \leq z \leq 1.4$); Pannella et al. (2009) use the COSMOS survey; Bolzonella et al. (2009) employ the zCOSMOS survey in the redshift range $0 < z < 1$; and Scodreggio et al.

(2009) investigate the environment dependence of the GMF based on the VVDS survey covering a redshift range of $0.2 < z < 1.4$.

On intermediate scales, $\sim h^{-1} \text{Mpc}$, groups and clusters of galaxies themselves provide a definition of environment. At low redshift, Balogh et al. (2001) using Two Micron All Sky Survey (2MASS) and Las Campanas Redshift Survey (LCRS) data, separate different environments as field, groups, and clusters, finding that galaxy luminosity and mass functions depend on both, galaxy type (with steeper functions for emission line galaxies) and mass of the group (with more massive and brighter objects more common in clusters), mainly as a consequence of the different contribution of passive galaxies (see also Hansen et al. 2009).

The environmental dependence of properties of gas is linked to the studies of warm-hot intergalactic media (WHIM). Hydrodynamical simulations by Cen & Ostriker (1999) show that the average temperature of baryons is an increasing function of time, with most of the baryons at the present time having a temperature in the range of $10^5 - 10^7 \text{K}$. The detection of this warm-hot gas poses an observational challenge. While according to their census more than one-half of the normal matter is yet to be detected, it is not clear which methods have to be used. In a later study Cen & Ostriker (2006) report that the gas density of the warm-hot intergalactic medium is broadly peaked at a density three to seven times the critical density, however their dark matter mass resolution was only moderate and a question of assigning baryons to groups has not been addressed.

All the above studies would greatly benefit from a

¹ Max Planck Institut für Astrophysik, Karl-Schwarzschild-Str. 1, 85741 Garching, Germany

² MPA/SHAO Joint Center for Astrophysical Cosmology at Shanghai Astronomical Observatory, Nandan Road 80, Shanghai 200030, China

³ Physics Department, University of the Western Cape, Cape Town 7535, South Africa

⁴ Max-Planck-Institut für Extraterrestrische Physik, Giessenbachstraße, 85748 Garching, Germany

⁵ University of Maryland, Baltimore County, 1000 Hilltop Circle, Baltimore, MD 21250, USA

quantification of the contribution of galaxy groups to the density fields as a function of background density. The significance of this question has been recognized before (e.g., Sheth & Tormen 1999), but a detailed answer has never been provided. Simulation work has instead concentrated on questions regarding halo assembly bias and, in particular, on changes in the properties of galaxies within the halos of similar mass but residing in different environments (Lemson & Kauffmann 1999; Gao et al. 2005; Croton et al. 2007).

This paper is organized as follows. In Section 2 we review the Millennium Simulation, the semi-analytic modeling of galaxies and the determination of the background density. Section 3 examines the dependence of the dark matter halo mass fractions on environment. In Section 4 halo mass functions in different environments are discussed. Section 5 focuses on the dependence of the GMFs on environment. We present a short summary in Section 6.

2. DATA

This analysis is based on the publicly available Millennium simulation run (MS; Springel 2005; Lemson & Springel 2006). In the first part of this section, we review the MS and the semianalytic galaxy modeling. The second part describes the determination of background densities and halo mass fractions.

2.1. Millennium simulation

The MS adopts concordance values for the parameters of a flat Λ cold dark matter cosmological model, $\Omega_{\text{dm}} = 0.205$ and $\Omega_{\text{b}} = 0.045$ for the current densities in cold dark matter and baryons, $h = 0.73$ for the present dimensionless value of the Hubble constant, $\sigma_8 = 0.9$ for the rms linear mass fluctuation in a sphere of radius $8 h^{-1}\text{Mpc}$ extrapolated to $z = 0$, and $n = 1$ for the slope of the primordial fluctuation spectrum. The simulation follows 2160^3 dark matter particles from $z = 127$ to the present day within a cubic region $500 h^{-1}\text{Mpc}$ on a side. The resulting individual particle mass is $8.6 \times 10^8 h^{-1}M_{\odot}$. The gravitational force has a Plummer-equivalent comoving softening of $5 h^{-1}\text{kpc}$. The Tree-PM N -body code GADGET2 (Springel et al. 2005) has been used to carry out the simulation and the full data are stored 64 times spaced approximately equally in the logarithm of the expansion factor.

The halos are found by a two-step procedure. In the first step, all collapsed halos with at least 20 particles are identified using a standard friends-of-friends (FoF) group-finder with linking parameter $b = 0.2$. These objects will be referred to as FoF-halos. Then, post-processing with the substructure algorithm SUBFIND (Springel et al. 2001) subdivides each FoF halo into a set of self-bound *sub-halos*. Based on their assembly histories, individual sub-halos are populated with galaxies by a semi-analytic prescription and various observable quantities are generated. For a detailed description of the semi-analytic galaxy catalog we refer the reader to Croton et al. (2006) and De Lucia & Blaizot (2007). The stellar mass functions in this study are based on the DeLucia2006a_SDSS2MASS catalog (Lemson & Virgo Consortium 2006, <http://www.g-vo.org/Millennium>).

The following analysis is based on FoF halos which

hereafter are addressed simply as halos. In principle, one also could use different halo definitions like those derived from spherical top-hat overdensity criteria or gravitational self-boundedness. The former would ease a comparison with observations and the latter would not suffer from the bridging problem inherent to the FoF approach. However, according to various tests which we have performed, the results based on the various halo identification schemes show little difference. The advantage of using FoF halos lies in the simplicity of the approach which makes it a very common tool for the analysis of N -body simulations.

2.2. Background Density and Halo/Galaxy Mass Fraction

The MS database also provides information on the global density field besides describing individual halo properties. Here, we use the densities, ρ_{CiC} , which are based on a Counts in Cell (CiC) approach using cubic cells of $\sim 2 h^{-1}\text{Mpc}$ on a side (Hockney & Eastwood 1988) and ρ_{G10} (hereafter *background density*), which are derived from the former by smoothing them with a $10 h^{-1}\text{Mpc}$ Gaussian kernel. In this study, we utilize ρ_{CiC} to compute the total amount of matter in a given volume and calibrate the use of the $10 h^{-1}\text{Mpc}$ background density fields, ρ_{G10} . We assume that ρ_{G10} represents the linear density field.

To determine the total mass of halos per cell, we reimplement the CiC approach only taking into account the particles belonging to FoF halos above a given mass limit. If a halo crosses the boundary of a cell, only the mass of the halo inside the cell is counted. This quantity is used to compute the halo *mass fractions* in Section 3.2. For the determination of the halo and the GMFs (Section 4 and Section 5), we attribute the total mass of halos or galaxies to the cell within which their centers are located. Eventually, each cell is assigned a total mass and in halos, a total mass in stars (galaxies), a total mass, and a smoothed background density (which after multiplication with the cell volume corresponds to a mass as well).

The upper left and the two lower panels of Figure 1 display a slice of the density contrast, $\delta_{\text{G10}} = (\rho_{\text{G10}} - \langle \rho \rangle) / \langle \rho \rangle$ scaled by the variance of the matter fluctuations within a volume corresponding to the Gaussian filter, σ_{G10} , at redshifts $z = 0$, $z = 1$, and $z = 3$. Typical patterns of the large-scale density field are apparent, such as roughly spherical high density regions, filaments, and voids. According to linear theory, δ/σ does not change with time. Indeed, the scaled density contrast is very similar in shape and amplitude at the redshifts we consider. Figure 2 shows the differential mass distributions as functions of the scaled density contrast. Red curves show the lognormal fits to the distribution (cf., Coles & Jones 1991; Neyrinck et al. 2009). The approximate invariability of the scaled contrast reaffirms the presumption of linearity of δ_{G10} .

The top right panel of Figure 1 shows the halo distribution within a slice of $10 h^{-1}\text{Mpc}$ thickness at $z = 0$ at the same location as slice used for the contrasts. The underlaid gray scale image is a replication of the contrast on the left. As expected, the halo distribution follows the pattern of the background density field. In the following, we measure the dependence of the fraction of mass captured in halos or galaxies as a function of the background

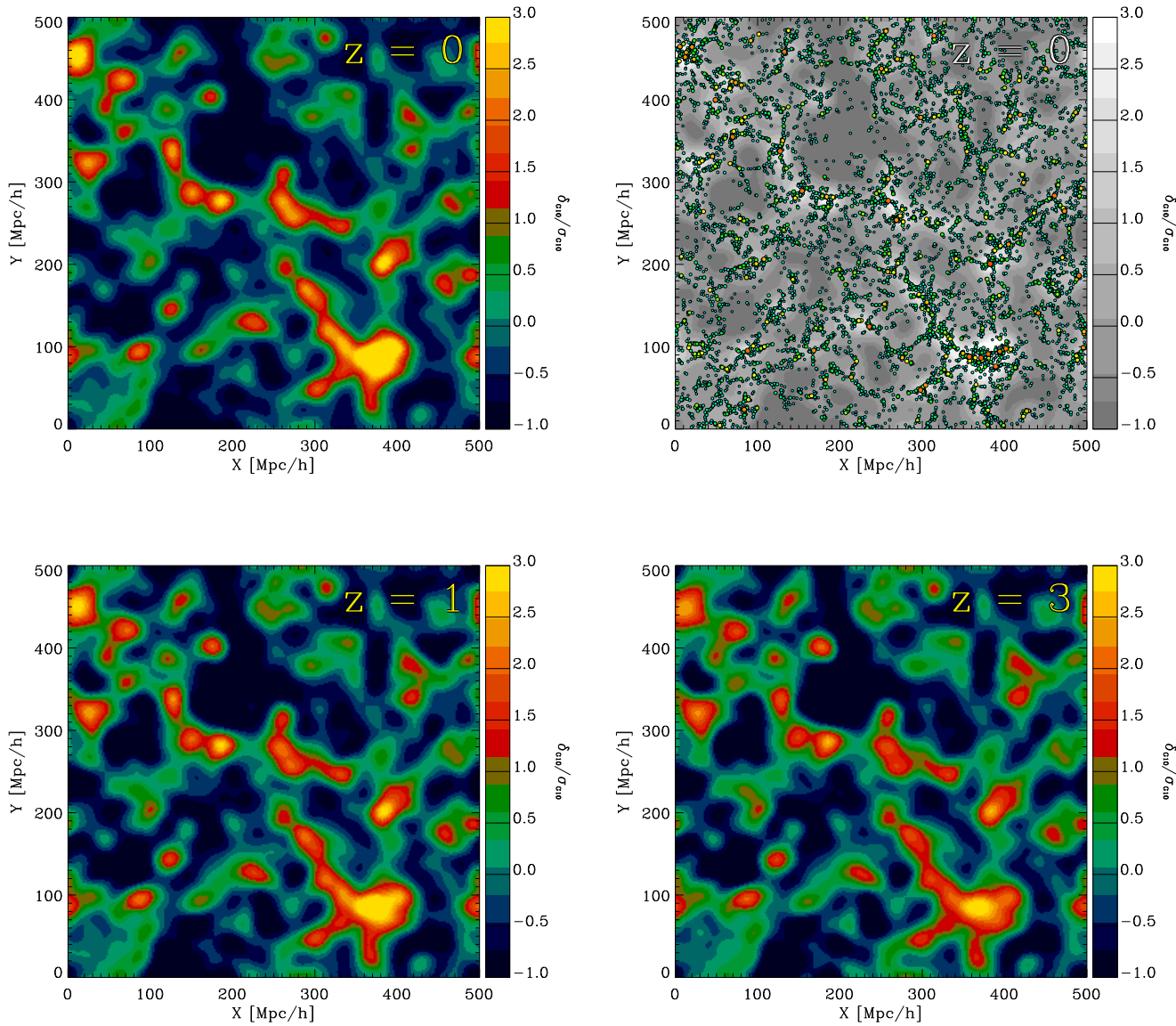


FIG. 1.— Upper left panel: dark matter density field at $z = 0$, smoothed using a Gaussian filter with a smoothing scale of $10 h^{-1} \text{Mpc}$, $\delta_{\text{G}10}$, and scaled by the average rms fluctuations within the corresponding volume, $\sigma_{\text{G}10}$. Upper right panel: density field as shown on the left in gray scale. The points represent halos above $10^{12} h^{-1} \text{M}_{\odot}$ within a slice of $10 h^{-1} \text{Mpc}$ thickness. Colors (from green to red) and sizes (from small to large) correspond to the logarithmic mass of the halos. As expected, the halo distribution closely follows the density field. Lower panels: smoothed and scaled density fields, as the upper left panel, but for the redshifts $z = 1$ and $z = 3$. According to linear theory δ/σ does not change with time.

density.

3. HALO MASS FRACTIONS

The first part of this section notes some general features associated with the characterization of the density field. In the subsequent paragraph, we examine the dependence of the halo mass fraction on environment. The *halo mass fraction* is defined as the mass locked in halos divided by the total mass in a given volume. As stated before, the environment is quantified based on the smoothed density within this volume. The halo mass fraction is closely related to the cumulative halo mass function which will be discussed in the subsequent section.

3.1. Mass within Isodensity Surfaces

The upper panel in Figure 3 shows the ratio between the average CiC-density of all cells located in regions of a given density contrast, $\delta_{\text{G}10}$, as a function of the density contrast itself. Line styles correspond to different redshifts. At a contrast of $\delta_{\text{G}10} \approx 0.2$, the mass within a cell approximately corresponds to the value of $\rho_{\text{G}10}$ multiplied by the cell volume. For higher contrasts, the actual mass deposited in the cell is larger than that deduced from the smoothed density field. The opposite is true for contrasts below 0.2. This behavior simply reflects that extremes are leveled by the smoothing procedure.

More important for the subsequent analysis is the lower panel in Figure 3. It displays the mean value of $\rho_{\text{CiC}}/\rho_{\text{G}10}$ within a volume confined by the isodensity

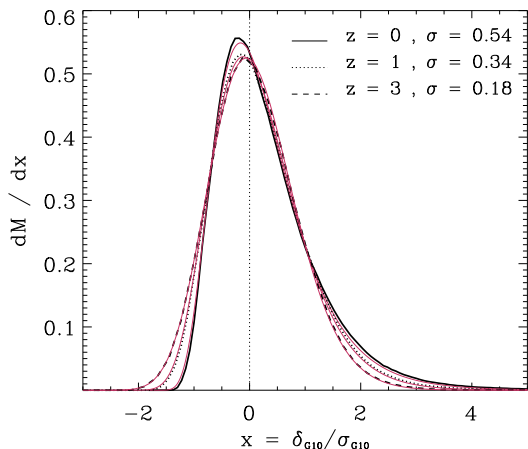


FIG. 2.— Differential mass distribution as a function of scaled density contrast. The density is computed based on a $10 h^{-1}$ Mpc Gaussian smoothing kernel, and the scaling factor, σ_{G10} , is the mass variance within a corresponding volume. Solid, dotted, and dashed lines indicate the redshifts $z = 0, 1$ and 3 , respectively. The red curves show the lognormal fits to the distribution.

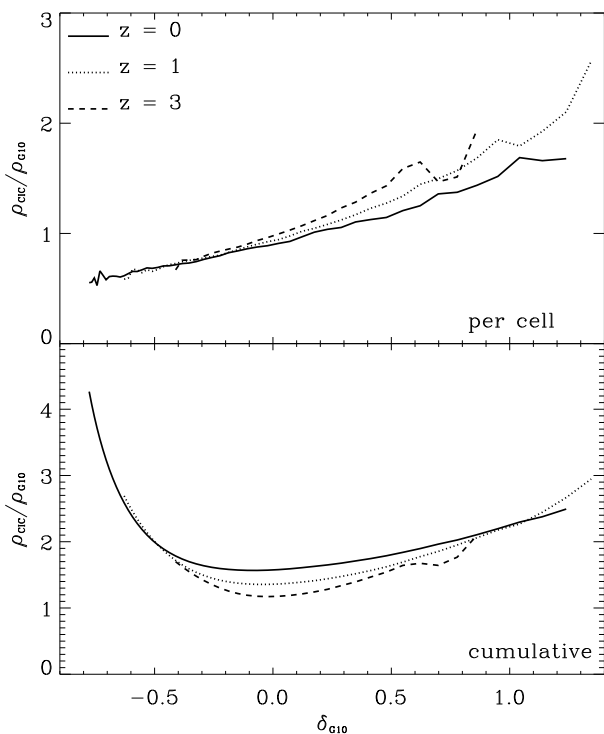


FIG. 3.— Upper panel: mean CiC density as a function of smoothed density. Lower panel: mean density within isodensity contours divided by that isodensity.

surface, ρ_{G10} , as a function of ρ_{G10} or its equivalent δ_{G10} . The ratio, ρ_{CIC}/ρ_{G10} , gives the average factor with which the confining density has to be multiplied to get the true mean density or the true mass within the enclosed volume. For different redshifts, indicated by different line styles, one finds slightly different ratios, but the overall behavior is similar. For density contrasts between 0 and 1.5, which are of interest here, one obtains $1 \lesssim \rho_{CIC}/\rho_{G10} \lesssim 3$. This factor has to be accounted for when the total mass within a given volume is inferred from the confining isodensity surface. Loosely speaking,

a factor of 2 has to be multiplied to the value of the confining surface density, ρ_{G10} , to recover the mass inside.

3.2. The dependence of the halo mass fraction on environment

The three panels in Figure 4 show the *halo mass fractions* for the redshifts $z = 0, z = 1$, and $z = 3$. The halo mass fraction is defined as the fraction of mass locked in halos (above a given limiting mass) and the total mass within a volume confined by isodensity surfaces with a density contrast δ_{G10} as a function of that contrast. Line styles refer to halo mass limits as indicated. For each redshift, these mass limits correspond to fixed values of the equivalent peak height, $\nu(M, z) = \delta_c(z)/\sigma(M, z)$, where $\sigma(M, z)$ is the rms linear overdensity within a sphere containing the mass M at redshift z , and $\delta_c(z)$ is the linear overdensity threshold for collapse at that redshift. The usage of ν instead of the actual halo mass should remove much of the cosmology dependence of our results and will be most useful for the discussion of the halo mass functions below. The mass limits for the left and middle panels correspond to $\nu \approx 0.9, 1.0, 1.2, 1.4, 1.7$, and 2.1 . In the $z = 3$ panel (on the right) mass resolution only allows us to show the graphs for the three highest ν values, 1.4, 1.7, and 2.1.

Figure 5 shows the fraction of mass in halos with respect to the total mass for confining density contrasts of $\delta_{G10} = 0.5, 1.0$ and 1.5 as a function of the mass limit of the halos. It is formally identical to the conditional cumulative mass function, $F(\nu)$, which is discussed in the next section. However, here it is computed based on the particle distributions of halos. Therefore, the mass of halos which transgress cell boundaries is accurately split between the cells. The analysis in the next section is somewhat more coarse in the sense that it attributes the total mass of a halo to only one cell, namely the cell where the center of the halo is located. This can introduce some bias, similar in origin to the deviation of surface and mean enclosed density discussed in 3.1. However, the comparison between the two methods yields acceptable agreement which implies confidence in the computation of the mass functions presented below.

3.3. Where are the Warm-Hot Baryons?

Our findings have consequences for the detection of warm-hot intergalactic baryons (WHIM). Cosmological simulations predict that some 50% of all the baryons locally appear in the form of gas with temperatures between 10^5 and 10^7 K (Cen & Ostriker 1999). The main process responsible for heating the baryons to such temperatures is large scale structure formation and thus the missing component is thought to be associated with high densities. Observational detection of this component became subject of a number of studies, and yet a full account of warm-hot baryons has not been reached.

In a subsequent study Davé et al. (2001) have argued that the major fraction of WHIM is located outside galaxy groups. Using hydrodynamical simulations they have shown that the total fraction of WHIM associated with galaxy groups is between 10% and 25%, depending on the group mass cut and that the majority of the WHIM resides at mean densities of $10 < \delta < 200$. In this work, no attempt has been undertaken to study the contribution of baryons in galaxy groups to the WHIM as a

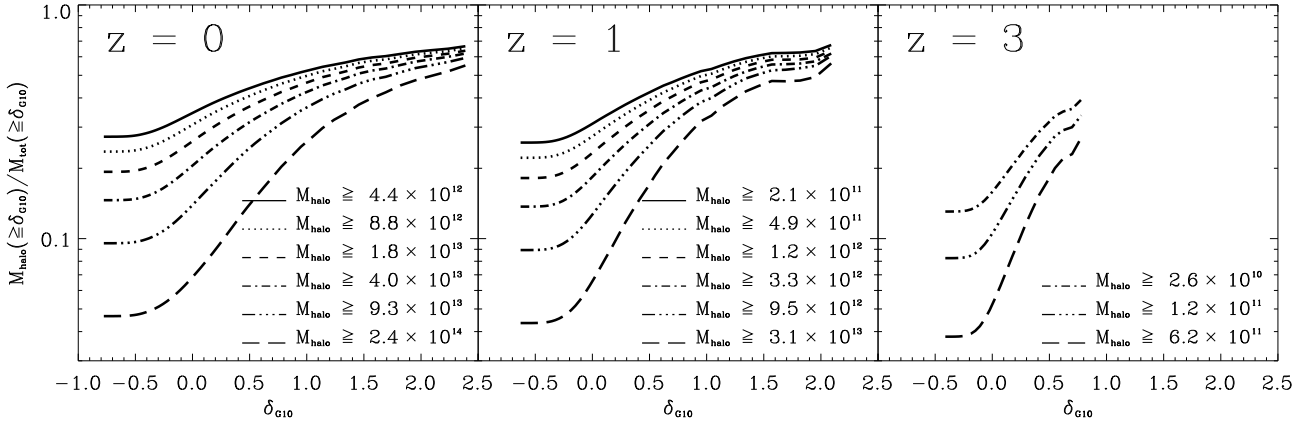


FIG. 4.— Halo to total mass fraction as a function of background density contrast, δ_{G10} . As indicated, the line styles correspond to different lower mass limits for the halos used to compute to total halo mass budget. For the left and middle panels, these masses correspond to the equivalent peak heights $\nu = 0.9, 1.0, 1.2, 1.4, 1.7, \text{ and } 2.1$. In the $z = 3$ panel on the right only the limiting masses corresponding to $\nu = 1.4, 1.7, \text{ and } 2.1$ are shown. At that redshift, ν -values below 1.4 correspond to halos with less than ~ 20 particles which are not resolved.

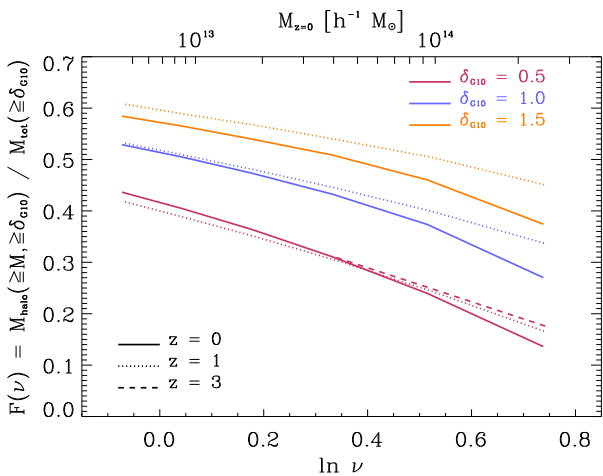


FIG. 5.— Conditional cumulative halos mass function, $F(\nu)$, i.e., fraction of mass locked in halos with respect to the total mass within a region confined by the contrasts, $\delta_{G10} = 0.5, 1.0, \text{ and } 1.5$ as a function of halo mass given parameterized by the equivalent peak height $\nu = \delta_c(z)/\sigma(M, z)$. The mass scale at the top indicates the equivalent masses for $z = 0$. Solid, dotted, and dashed lines correspond to redshifts $z = 0, 1, \text{ and } 3$, respectively. At $z = 3$ δ_{G10} does not reach 1.

function of environment. Here we aim to determine the fraction of WHIM located in groups at high background densities.

Figure 4 suggests a dominant contribution of groups to the matter budget at high overdensities, resolving 60% of total mass in groups with mass exceeding $2 \times 10^{13} M_\odot$ and 70% of total mass in groups with mass exceeding $4 \times 10^{12} M_\odot$. Without any background density restriction these groups account for 20%–30% of matter.

It is important to note that no gas component has been included in the Millennium Simulation. To derive conclusions on the WHIM, we rely on a model describing the distribution of gas relative to the overall matter distribution which is equivalent to dark matter distribution in the current context. Here, we assume for simplicity that gas follows dark matter. Hydrodynamical simulations show that this assumption is well justified for local densities below $\lesssim 10^4$ times the cosmic mean density (Faltenbacher et al. 2007, cf., []). Furthermore, observational and theoretical accounts for baryons in-

side groups indicate that the universal baryon fraction is nearly recovered (Kravtsov et al. 2005; Sun et al. 2009; Giodini et al. 2009; McGaugh et al. 2010), and potentially can be fully resolved by accounting the baryons near the virial radius. Thus, on the supposition that gas follows the dark matter our findings indicate that 20%–30% of the WHIM is located in groups if no background density constraint is imposed, whereas 60%–70% of the WHIM is residing in galaxy groups at high background densities. The former agrees well with the figures quoted in Davé et al. (2001).

The only observational result published on the global fraction of mass in groups, by Reiprich & Böhringer (2002), uses *ROSAT* All Sky Survey data, and quoted $\Omega_{cluster} = 0.012$ (or 5% contribution of clusters to the total mass budget) for masses exceeding $10^{14} M_\odot h^{-1}$. This measurement compares well with our value for $M > 2 \times 10^{14} h^{-1} M_\odot$, which corresponds to the same ν when a difference in the σ_8 value between observed universe and the Millennium run is taken into account. This account will likely improve soon since current X-ray surveys can access masses below $10^{13} M_\odot$ (Finoguenov et al. 2007, 2009). Also, detections of WHIM in X-ray emission regions agree well with our findings at high background densities. For example, Werner et al. (2008) find that most masses of baryons in the A222/A223 complex are locked within the halos, with WHIM contributing 10%–20%.

At this point we would like to emphasize that the definition of densities adopted in WHIM studies is different from that one used here. Our results constrain the WHIM aspect within the definition of density fields typical to spectroscopic surveys (e.g., Kovač et al. 2010). In contrast the computation of the local density of the Lyman α absorbers can only be derived from their HI column densities, resulting in a non-trivial role played by the absorber’s size and shape. In Penton et al. (2004) the first comparison to LSS density has been provided, showing the half of the absorbers reside in voids.

Figure 4 limits the importance of the WHIM component in regions of high density (as defined on a 10 Mpc scale) which is not associated with groups to 30%. Therefore, the situation is much more favorable toward detecting missing baryons in underdense regions, but there

the temperature of the gas will be quite low. In fact the major success in resolving the missing baryons has been achieved using techniques looking for colder gas (Penton et al. 2004).

4. CUMULATIVE HALO MASS FUNCTIONS

Up to this point, we have used the particle distribution of the halos to split their mass among the cells they occupy. In the following we use the halo position to attribute the entire halo mass to one cell. This reduces the accuracy of the determination of the mass fraction slightly ($\lesssim 5\%$). However, that way the treatment of halos and model galaxies which are examined hereafter and have unknown spatial extent can be matched.

Plenty of studies have been devoted to investigate the mass function of halos in the cosmological context. Early analytical approaches suggested that the mass function is universal, i.e. its shape is independent of time and background cosmology if adequate variables are used. In a seminal study, Press & Schechter (1974) used the equivalent peak height, $\nu = \delta_c/\sigma$ (see also, Bond et al. 1991; Lee & Shandarin 1998; Sheth & Tormen 1999). Such models can help gain insight into the statistics of gravitational collapse. However, these highly nonlinear processes are complex, and a final validation of the models can only be obtained by direct comparison to numerical simulations. Based on N -body simulations, Jenkins et al. (2001) and Evrard et al. (2002) presented fitting formulae for the differential mass functions accurate to $\sim 10\% - 20\%$. These studies supported the view that mass functions are indeed universal. Also, the results obtained by Lukić et al. (2007) are consistent with a universal mass function; however, they report a mild redshift dependence at low redshifts (see also Reed et al. 2003). Warren et al. (2006) found a fitting formula accurate to $\sim 5\%$ for a fixed cosmology at $z = 0$. Recently, however, based on a large set of N -body simulations with different cosmological parameters Tinker et al. (2008) revealed that the mass function can not be represented by a universal mass function at this level of accuracy. In particular they found that the amplitude of the mass function decreases monotonically by $\approx 20\% - 50\%$ from $z = 0$ to $z = 2.5$. Several studies explore the mass functions at high redshifts (e.g., Reed et al. 2007; Cohn & White 2008) but they do not particularly focus on universality.

In general, analytical and numerical studies preferentially discuss the (unconditional) differential mass function. For our purposes the integrated form, i.e. the unconditional cumulative halo mass function (UHMF) is more useful since it directly gives the fraction of mass in halos relative to the total mass. Additionally, the functional forms of the unconditional differential mass functions, as given in the literature, are complex and their integrals are even more so. Thus, for our purposes it seems to be a better strategy to directly examine the cumulative mass function and derive a simple fitting function for it. Consequently, in the first part of this section we introduce a fitting function for the UHMFs. In the second part, this function is modified to be applicable for the cumulative mass functions at different background densities, hereafter referred to as conditional cumulative halo mass functions (CHMFs).

4.1. Unconditional Cumulative Halo Mass Functions

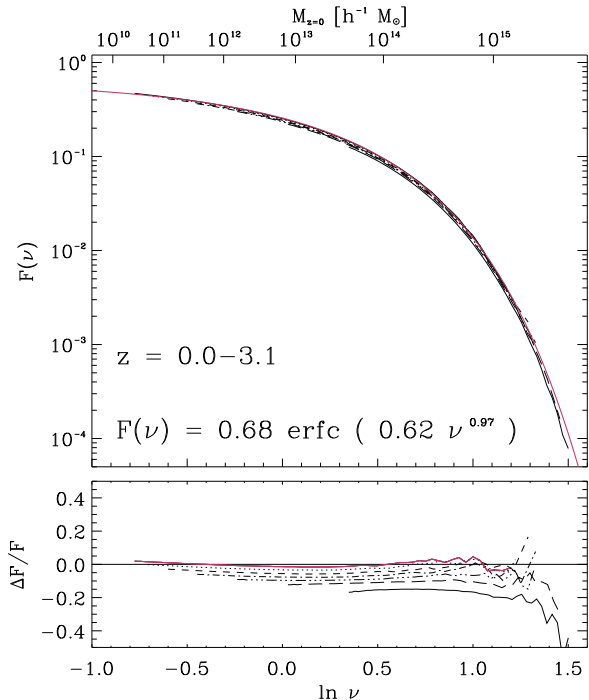


FIG. 6.— Upper panel: cumulative mass functions for redshifts $z = 0.00, 0.14, 0.36, 0.69, 1.17, 1.91,$ and 3.06 shown as solid, dotted, dashed, dot-dashed, three-dot-dashed, and solid lines, respectively. Halo mass is given parametrically through the equivalent peak height $\nu = \delta_c/\sigma$. At the top the corresponding mass scale for $z = 0$ is indicated. The red line presents a fit for the mass function at $z = 0$. The fitting function including the parameters is quoted in the bottom line. Lower panel: residuals of the mass functions and the fit at $z = 0$. The red line displays the residual for the mass function at $z = 0$ which has been used for fitting. An accuracy of $\lesssim 5\%$ is achieved for halo masses between 10^{10} and $10^{15} h^{-1} M_\odot$.

Under the assumption that the initial density field is a Gaussian random field and the validity of the spherical collapse model, Press & Schechter (1974) derived the mass fraction locked in halos above a given mass to the total mass in the universe,

$$F_{\text{PS}}(\nu) = \text{erfc}\left(\frac{\nu}{\sqrt{2}}\right), \quad (1)$$

where ν is the equivalent peak height as discussed in § 3.2, which, for a given cosmology, can be uniquely transformed into a corresponding halo mass, M . $F(\nu)$ is equivalent to the UHMF as introduced above. Press & Schechter (1974) argued that this parameterization makes the mass function universal, i.e. independent of evolutionary changes and cosmological parameters which are covered by the time and cosmology dependence of ν . Over the last 20 years, high-resolution N -body simulations demonstrated that Equation 1 reproduces the numerical halo mass function qualitatively. However, certain systematic deviations became apparent (e.g., Sheth & Tormen 2002; Warren et al. 2006; Tinker et al. 2008). Compared to N -body results, Equation 1 produces too many halos with masses corresponding to $\nu = 1$ and to few at the high mass end. Nevertheless, we use the functional form of Equation 1 as template for our fitting formula:

$$F_{\text{fit}}(\nu) = A \text{erfc}(a \nu^b), \quad (2)$$

with the fitting parameters A , a , and b . The upper panel of Figure 6 displays UHMFs for FoF halos derived from

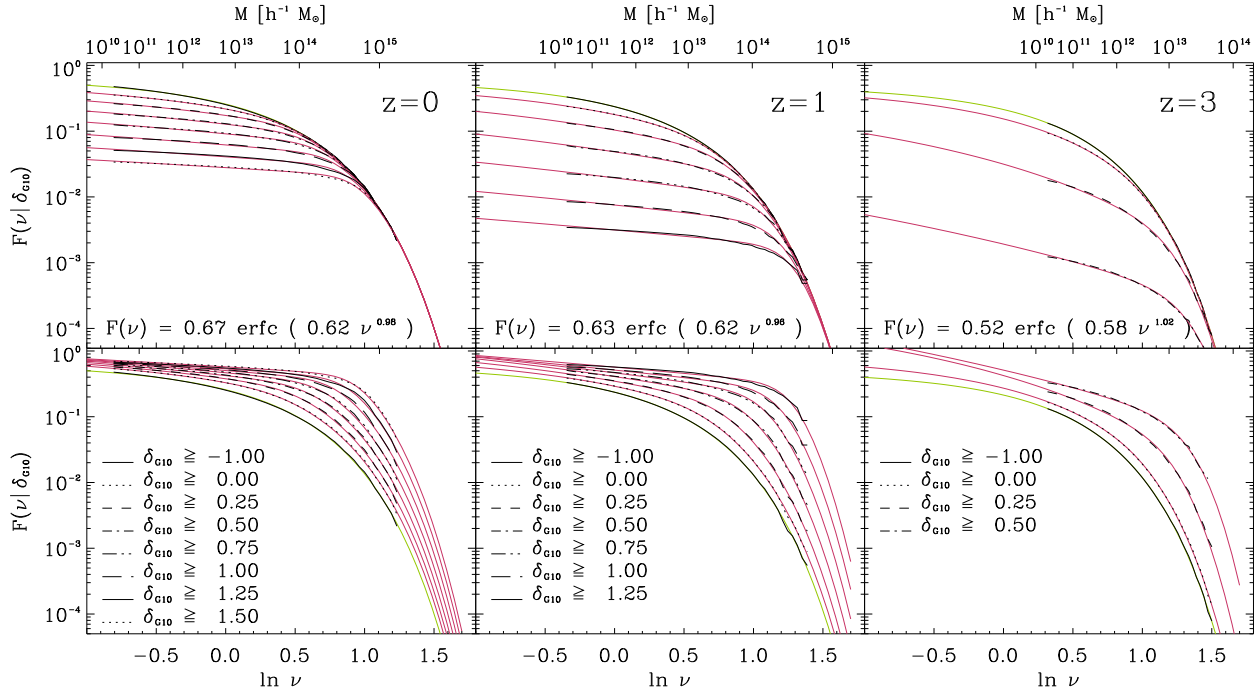


FIG. 7.— Dependence of the halo mass fraction on environment for the redshifts $z = 0, 1,$ and 3 . Lines styles correspond the CHMFs in regions confined by the density contrasts, δ_{G10} as indicated. Green lines represent a fits to the UHMF using Eq. 2. The fitting parameters are displayed at the bottom of the upper panels. Red lines show fits for the CHMFs using the fitting procedure described in Section 4.2. The only difference between the upper and lower panels is the mass normalization. In the upper panels, F gives the halo mass fraction with respect to the total mass in the box and in the lower panels with respect to the total mass enclosed in the overdense regions.

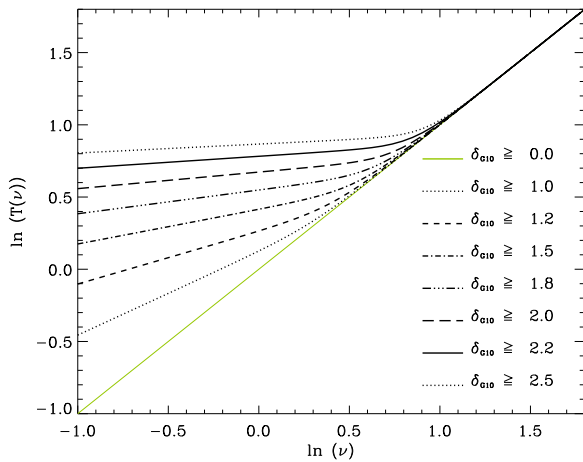


FIG. 8.— Coordinate transformation used to convert unconditional into conditional mass functions for the indicated density contrasts. To guide the eyes the green line for $\delta_{G10} = 0$ displays the identity. For higher contrasts, this transformation keeps the mass function for large values of $\ln(\nu)$ unchanged yet it causes the mass function at low $\ln(\nu)$ to level off.

the MS. Different line styles represent UHMFs derived from snapshots at redshift $z = 0.00, 0.14, 0.36, 0.69, 1.17, 1.91,$ and 3.06 . The red line shows a fit to the UHMF at $z = 0$. The corresponding fitting parameters are given in the panel. For the computation of the halo masses, we applied the correction formula proposed by Warren et al. (2006): $N_{\text{corrected}} = N(1 - N^{-0.6})$, where N denotes the number of particles within a given FoF halo. This correction is most effective at the low mass end. The fitting range is confined by FoF halos with masses between $2 \times 10^{10} h^{-1} M_{\odot}$ (200 particles) and $10^{15} h^{-1} M_{\odot}$.

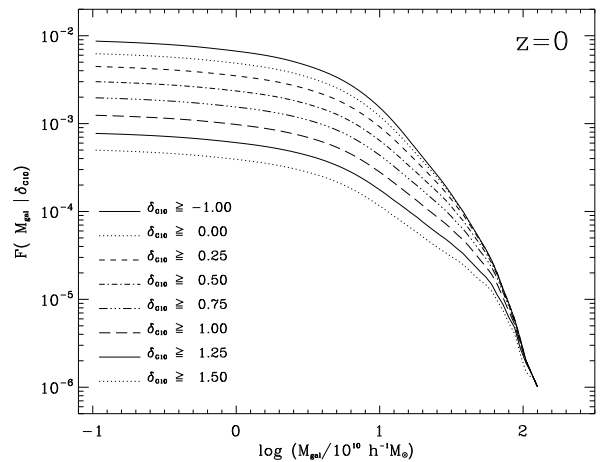


FIG. 9.— Environmental dependence of the cumulative galaxy mass function. Except for the usage of galaxy masses instead of halo masses the plot is equal to the upper left panel in Figure 7; the line styles are adopted from there as well.

The lower panel of Figure 6 shows the residuals between the UHMFs at the given redshifts and the fit based on the $z = 0$ mass function. The red line highlights the residual between the fit and the $z = 0$ mass function. At $z = 0$ and for masses in the range between $10^{10} h^{-1} M_{\odot}$ and $10^{15} h^{-1} M_{\odot}$, the fit is accurate to the 5% level. However, we note an increasing offset with redshift which results in a deviation of 15% at $z = 3.06$. Similar findings have been reported in Tinker et al. (2008). The expression, Equation 6, is an excellent fitting function for the cumulative mass function at $z = 0$. It is “universal”, i.e., independent of cosmology at a degree to which the parameterization by the equivalent peak height, ν , permits.

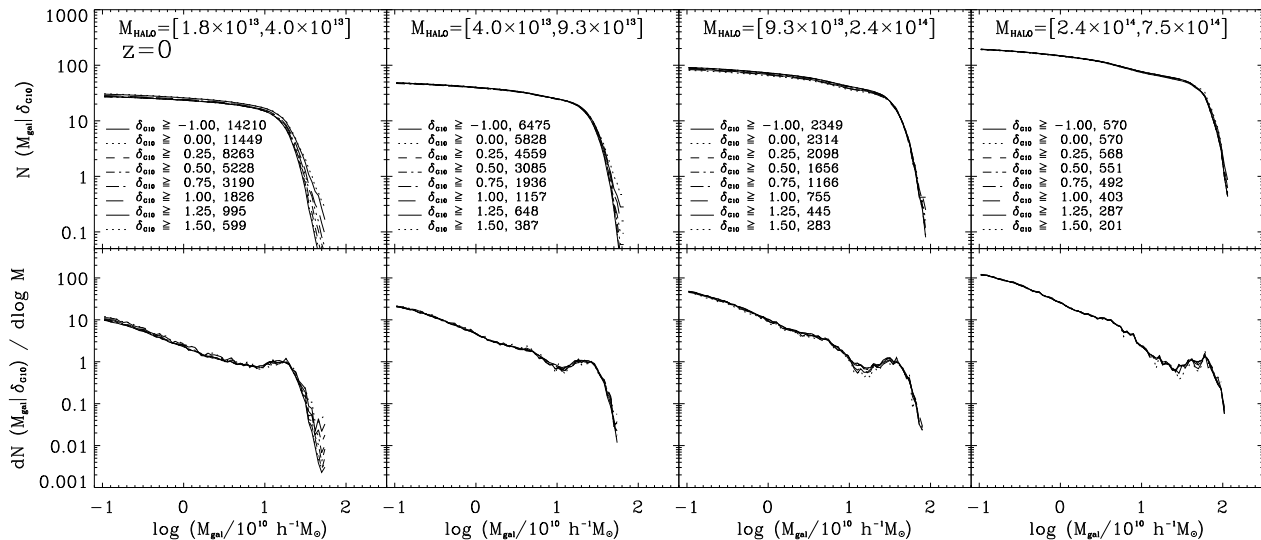


FIG. 10.— Upper panel: cumulative galaxy mass function in galaxy groups in different environments. Lower panel: differential galaxy mass function in galaxy groups in different environments. On each panel, we denote both the density field and the number of embedded groups.

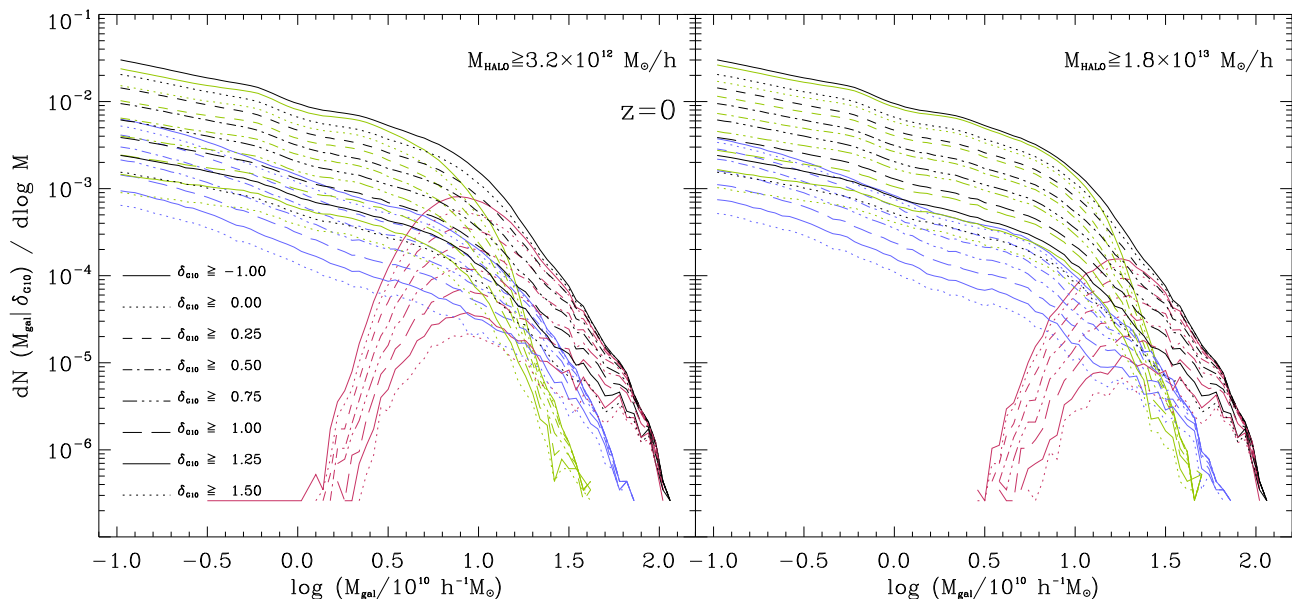


FIG. 11.— Differential galaxy mass function in different environments (black lines) separating the contribution of central (red lines) and non-central galaxies (green lines) in groups above the masses indicated in the upper right corner of the panels. The green lines show the contribution of galaxies not belonging to those groups. The particular role of the central galaxies is that they provide a hump-like contribution to the mass function and explain a variation of that hump with the environment.

4.2. Conditional Cumulative Halo Mass Function

The term “conditional mass function” has been used to address two related problems: (1) to describe the mass distribution of progenitor halos which end up in a given halo at later times; (2) to refer to the mass distribution of halos within a region of a given background density (cf., Mo & White 1996; Sheth 1998; Sheth & Lemson 1999; Sheth & Tormen 2002). Here we will investigate the latter. According to excursion set theory, the basic equation to approach such problems is

$$F(M|\delta_0, \sigma_0) = \text{erfc} \left(\frac{1}{\sqrt{2}} \frac{\delta_c - \delta_0}{\sigma - \sigma_0} \right), \quad (3)$$

where δ_c and σ are the same as used in Equation 1 and δ_0 and σ_0 are the linear density contrast and the dispersion of the background density field. It gives the fraction of mass in collapsed halos of mass greater than M (corresponding to $\nu = \delta_c/\sigma$) in a region that has a linear density contrast δ_0 (for a comprehensive review including references see, Zentner 2007). In the current context, two difficulties arise when this equation is to be applied. First, the boundary surface and hence the volume of the overdense regions can be quite irregular which makes it difficult to determine σ_0 appropriately. Second, to facilitate the comparison with observations, we intend to compute the mass fraction within regions *above* a given δ_{lim} , in other words cumulative with respect to the back-

Redshift	δ_{G10}	Δ	a	b	f_M
$z = 0$	0.00	1.00	1.00	1.00	1.00
	1.00	0.58	7.76	0.28	1.51
	1.25	0.36	7.90	0.41	2.18
	1.50	0.24	8.45	0.55	3.30
	1.75	0.16	8.91	0.66	5.12
	2.00	0.11	9.77	0.76	8.16
	2.25	0.08	10.25	0.85	13.17
	2.50	0.06	10.87	0.92	20.55
$z = 1$	0.00	1.00	1.00	1.00	1.00
	1.00	0.61	7.58	0.51	1.63
	1.25	0.34	7.28	0.71	3.34
	1.50	0.20	7.79	0.90	8.41
	1.75	0.12	8.69	1.05	23.86
	2.00	0.07	8.72	1.17	67.96
	2.25	0.05	10.18	1.27	180.57
$z = 3$	0.00	1.00	1.00	1.00	1.00
	1.00	0.74	7.37	0.91	1.77
	1.25	0.32	7.27	1.20	13.43
	1.50	0.12	6.18	1.41	266.83

TABLE 1

CHMF FITTING PARAMETERS, Δ, a, b AND MASS FACTOR f_m FOR THE BACKGROUND DENSITIES, δ_{G10} , AND REDSHIFTS $z = 0, 1,$ AND 3 .

ground density. However Equation 3 gives the halo mass fraction *at* a given δ_0 . Therefore, obtaining an expression suitable for our purposes would require an integration of Equation 3 with respect to δ_0 . This integration leads to a lengthy expression, which is too complex to be used as a model for a fitting formula (as done for the UHMF in Section 4.1).

Therefore, we choose a more phenomenological approach starting with the inspection of Figure 7. Black lines display UHMFs and CHMFs in regions above a given density contrast at redshifts of $z = 0, z = 1,$ and $z = 3$. The CHMFs are determined by summing up the mass of halos which reside in cells above a given contrast δ_{G10} . The difference between the upper and lower panels is only in normalization. In the upper panels, we use the total mass in the box whereas in the lower panels we use the total mass within the cells above δ_{G10} . Therefore, the CHMFs in the upper panels lie systematically below the UHMFs; this is because a fraction of the total volume is excluded by the density criterion – and so are the halos in it – but the mass fraction is still computed with respect to the total mass in the box. In the lower panels, the CHMFs lie systematically above the UHMFs which is a result of the decreasing total mass in the volume above the given background density. The latter is more physical but the former illustrates the fact that at the high-mass end all CHMFs display the same behavior as the UHMF. The green lines show fits to the UHMF. The values of the fitting parameters are given at the bottom of the upper panels (here the UHMFs are fitted separately for each redshift). The red lines are fits to the CHMFs.

Guided by the behavior seen in the upper panels of Figure 7, we conceive a fitting formula for the CHMFs which is based on a parameter-dependent coordinate transformation, $T(\nu)$, such that for an adequate set of parameters $F(T(\nu))$ (here F denotes the UHMF) matches a given CHMF. We use the following functional form for these transformations, constructed to map high ν values

onto themselves but narrowing the range for low ν s:

$$\ln(T(\nu)) = \Delta + \frac{ax + (1.0 - a) \ln[1.0 + \exp(x)]}{b}, \quad (4)$$

where $x = b (\ln(\nu) - \Delta)$. The values for the three parameters $\Delta, a,$ and b are listed in Table 1 with the corresponding fits shown as red lines in Figure 7. Figure 8 illustrates the coordinate transformations at $z = 0$. Δ determines where the deviation from one-to-one correspondence takes place, a gives the left hand side slope and b defines the smoothness of the transition between the two slopes. So far, we have described how to fit the CHMFs in the upper panels of Figure 7. To get the mass normalization right, i.e., to transform the fits of the upper panels into the those of the lower panels, these $F(T(\nu))$ have to be multiplied by the mass factor f_M which is listed in the rightmost column of Table 1. It gives the ratio of the total mass in the box to the mass confined to the considered overdense regions.

Our findings may help to illustrate some of the main mechanisms shaping the halo mass functions in different environments. The top heavy shape of the CHMFs is caused by a relative lack of small mass halos at high background densities. For our way of parameterizing the background density, namely, by using isodensity surfaces to indicate all the volume interior to it, the shape of the cumulative mass functions at the high mass end is independent of environment. The only difference is induced by the normalization which reflects the mass confined to the high density regions. It causes the amplitude of the mass function to rise.

As a concluding remark we note that the use of cumulative instead of differential mass functions proved valuable to extract these results. First, because it directly gives the fraction of mass in halos above a given mass with respect to the total mass. In addition, it's shape is simple compared to the differential mass function which eases finding a suitable fitting strategy. Finally, it allows us to easily derive some of its basic properties by analytically. For instance, it is obvious that the “wrongly normalized” CHMFs in the upper panels must coincide at the high mass end. Similarly easy to derive is that the fits in the lower panels must be confined by 1 even for extrapolations to smallest halo masses. The fact that this is obviously not the case for two of the $z = 3$ fits demonstrates the limits of the fitting procedure. However, in general the fits behave well, i.e., the amplitudes remain < 1 even if extrapolated to small masses.

5. CONDITIONAL GALAXY MASS FUNCTION

The semi-analytical modeling of galaxies included in the MS database (De Lucia & Blaizot 2007; Lemson & Virgo Consortium 2006) provides stellar masses for each model galaxy. This allows us to compute the conditional cumulative galaxy stellar mass function (CGMF) in exactly the same way as the CHMFs have been determined, namely by summing up the mass of all galaxies which reside in cells above a given contrast δ_{G10} . We set the lower limit for the galaxy masses to $10^9 h^{-1} M_\odot$. Figure 9 shows the results of the CGMF normalized by the total mass in the box, which is the reason why all mass functions coincide at the high-mass end, equivalently to the behavior of the CHMFs. In general, the changes in CGMF

are qualitatively very similar to that of the CHMFs: becoming top heavy at high background densities.

The qualitative similarities between the CHMFs and CGMFs suggest that the dependence of the model galaxy mass function on environment is caused by the corresponding dependence of the halo mass function on environment, rather than on direct impact of environment on galaxy evolution (generally referred to as nurture effects). To test this conjecture, Figure 10 shows the model galaxy mass functions at different background densities with the additional restriction that they reside in dark matter halos of a given mass range as indicated by the labels right on top. The upper panels show the cumulative galaxy mass functions and the lower panels depict the GMF in differential form. The line styles correspond to different density thresholds listed in the figure. The integer numbers indicate the number of halos in those regions. Evidently, these numbers show a strong dependence on environment assuring that the galaxy mass functions displayed in a single panel are based on very different sets of host halos. Nevertheless, the resulting mass functions deviate by less than 10% for galaxy masses $\lesssim 10^{11} h^{-1} M_{\odot}$. Therefore, the large changes in the CGMFs can almost entirely be accounted for by changes in the host halo population. Nurture effects may have a minor impact on shaping the model galaxy mass function in different environments.

There are some shortcomings in the semianalytical model of galaxy formation used here (De Lucia & Blaizot 2007). The two most important are: (1) cooling is instantaneously shut down for galaxies whose halo enters a larger one; (2) tidal forces are not allowed to strip off stars reducing the luminosity of a given galaxy. Nevertheless, these processes do mostly affect satellite galaxies. Thus, we believe that the behavior seen at the high mass end of the CGMFs should be a reliable prediction from the semianalytical model.

To provide a further illustration, we display the differential galaxy mass function as a function of environment separating the contribution of central and non-central galaxies in groups in Figure 11. The particular role of central galaxies is that they provide a hump-like contribution to the mass function and illustrate the variation of that hump with the environment, therefore explain another important observational result (e.g., Bolzonella et al. 2009). Explaining the hump-like feature as being due to the contribution of central galaxies (and hence a bimodal GMF with centrals and satellites as its two constituents) is somewhat different than the explanation given by Bolzonella et al. (2009), namely that the hump is due to the contributions of red galaxies to the total GMF. In our view, the hump is a consequence of halo assembly, not of the transformation of blue into red galaxies, although the two processes might be linked in the sense that the assembly of central galaxies might also lead to quenching of their star formation in some halos. We therefore predict that the hump will also be seen in the blue galaxy mass function alone, not only in the total GMF, since many halos host giant (blue) spiral galaxies as their central galaxy. Indeed, this bimodality in the blue galaxy mass function has been observed by

Drory et al. (2009).

The thermodynamical state of the accreting gas is expected to vary with redshift, enabling a cold accretion at $z > 2$ and subsequent star formation in the central galaxy even in halos as massive as $10^{13} M_{\odot}$ (Dekel et al. 2009). These are expected to be the highest peaks of density field at those redshifts and therefore obey our predictions for the behavior in high density environments. Observational search for the transitional halo mass between the cold and the hot accretion mode is difficult, as this mass is well below the sensitivity of both spectroscopic and X-ray surveys for defining the galaxy groups. Instead, here we propose to use the shape of the galaxy mass function to determine at which halo mass the transition occurs. Since the central galaxies of groups make a hump-like contribution to the galaxy mass function, the blue central galaxies should constitute a blue hump. The location of the blue hump in the galaxy mass function can therefore be used through a comparison to numerical simulations to determine the transition halo mass scale for shutting down the star formation or environmental dependence of cold accretion mode in galaxy formation. In contrast to clustering studies, the proposed method does not induce a requirement on the data to be representative, and can therefore be applied to a field of any size or even a selected object, like a high-redshift supercluster.

6. CONCLUSIONS

Using the Millennium Simulation and current schemes for density field reconstruction, we parameterize the conditional halo mass function. As an application, we consider the role of halos in explaining the missing baryon problem and the environmental dependence of galaxy mass functions. We show that in high-density environments galaxy groups provide a major contribution to total matter content. We discuss the implication of this result for search of missing baryons. Under the well-justified assumption that baryons follow dark matter, we show that its amount can be constrained using the observations of galaxy groups. We also point out that the environmental changes in galaxy mass functions are caused by changes in mass function of groups and, in particular, that a hump-like features in galaxy mass function is produced by the central galaxies of groups.

ACKNOWLEDGMENTS

The authors are thankful to the anonymous referee for insightful suggestions, to Simon White for valuable comments on the paper and to Eyal Neistein for helpful discussions. Andreas Faltenbacher is supported by the SA SKA bursary program and acknowledges the kind hospitality at South African Astronomical Observatory. Alexis Finoguenov acknowledges support from *Spitzer* UDS Legacy program to UMBC. The Millennium Simulation databases used in this paper and the web application providing online access to them were constructed as part of the activities of the German Astrophysical Virtual Observatory. The authors thank Gerard Lemson for his help with MS database and the comments on the manuscript.

REFERENCES

- Baldry, I. K., Balogh, M. L., Bower, R. G., Glazebrook, K., Nichol, R. C., Bamford, S. P., & Budavari, T. 2006, MNRAS, 373, 469
- Balogh, M. L., Christlein, D., Zabludoff, A. I., & Zaritsky, D. 2001, ApJ, 557, 117

- Bolzonella, M., Kovac, K., Pozzetti, L., Zucca, E., Cucciati, O., Lilly, S. J., Peng, Y., Iovino, A., & et al. 2009, ArXiv e-prints; 0907.0013
- Bond, J. R., Cole, S., Efstathiou, G., & Kaiser, N. 1991, *ApJ*, 379, 440
- Bundy, K., Ellis, R. S., Conselice, C. J., Taylor, J. E., Cooper, M. C., Willmer, C. N. A., Weiner, B. J., Coil, A. L., & et al., 2006, *ApJ*, 651, 120
- Cen, R. & Ostriker, J. P. 1999, *ApJ*, 514, 1
- . 2006, *ApJ*, 650, 560
- Cohn, J. D. & White, M. 2008, *MNRAS*, 385, 2025
- Coles, P. & Jones, B. 1991, *MNRAS*, 248, 1
- Colless, M., Dalton, G., Maddox, S., Sutherland, W., Norberg, P., Cole, S., Bland-Hawthorn, J., Bridges, T., & et al. 2001, *MNRAS*, 328, 1039
- Croton, D. J., Gao, L., & White, S. D. M. 2007, *MNRAS*, 374, 1303
- Croton, D. J., Springel, V., White, S. D. M., De Lucia, G., Frenk, C. S., Gao, L., Jenkins, A., Kauffmann, G., & et al., 2006, *MNRAS*, 365, 11
- Davé, R., Cen, R., Ostriker, J. P., Bryan, G. L., Hernquist, L., Katz, N., Weinberg, D. H., Norman, M. L., & et al., 2001, *ApJ*, 552, 473
- De Lucia, G. & Blaizot, J. 2007, *MNRAS*, 375, 2
- Dekel, A., Birnboim, Y., Engel, G., Freundlich, J., Goerdt, T., Mumcuoglu, M., Neistein, E., Pichon, C., & et al., 2009, *Nature*, 457, 451
- Dressler, A. 1980, *ApJ*, 236, 351
- Drory, N., Bundy, K., Leauthaud, A., Scoville, N., Capak, P., Ilbert, O., Kartaltepe, J. S., Kneib, J. P., & et al., 2009, *ApJ*, 707, 1595
- Evrard, A. E., MacFarland, T. J., Couchman, H. M. P., Colberg, J. M., Yoshida, N., White, S. D. M., Jenkins, A., Frenk, C. S., & et al., 2002, *ApJ*, 573, 7
- Faltenbacher, A., Hoffman, Y., Gottlöber, S., & Yepes, G. 2007, *MNRAS*, 376, 1327
- Finoguenov, A., Connelly, J. L., Parker, L. C., Wilman, D. J., Mulchaey, J. S., Saglia, R. P., Balogh, M. L., Bower, R. G., & et al., 2009, *ApJ*, 704, 564
- Finoguenov, A., Guzzo, L., Hasinger, G., Scoville, N. Z., Aussel, H., Böhringer, H., Brusa, M., Capak, P., & et al., 2007, *ApJS*, 172, 182
- Gao, L., Springel, V., & White, S. D. M. 2005, *MNRAS*, 363, L66
- Godini, S., Pierini, D., Finoguenov, A., Pratt, G. W., Böhringer, H., Leauthaud, A., Guzzo, L., Aussel, H., & et al., 2009, *ApJ*, 703, 982
- Hansen, S. M., Sheldon, E. S., Wechsler, R. H., & Koester, B. P. 2009, *ApJ*, 699, 1333
- Hockney, R. W. & Eastwood, J. W. 1988, *Computer simulation using particles*, ed. J. W. Hockney, R. W. & Eastwood
- Jenkins, A., Frenk, C. S., White, S. D. M., Colberg, J. M., Cole, S., Evrard, A. E., Couchman, H. M. P., & Yoshida, N. 2001, *MNRAS*, 321, 372
- Kovač, K., Lilly, S. J., Cucciati, O., Porciani, C., Iovino, A., Zamorani, G., Oesch, P., Bolzonella, M., & et al., 2010, *ApJ*, 708, 505
- Kravtsov, A. V., Nagai, D., & Vikhlinin, A. A. 2005, *ApJ*, 625, 588
- Lee, J. & Shandarin, S. F. 1998, *ApJ*, 500, 14
- Lemson, G. & Kauffmann, G. 1999, *MNRAS*, 302, 111
- Lemson, G. & Springel, V. 2006, in *Astronomical Data Analysis Software and Systems XV*, ed. C. Gabriel, C. Arviset, D. Ponz, & S. Enrique, Vol. 351, 212–+
- Lemson, G. & Virgo Consortium, t. 2006, ArXiv Astrophysics e-prints, astro-ph/0608019
- Lukić, Z., Heitmann, K., Habib, S., Bashinsky, S., & Ricker, P. M. 2007, *ApJ*, 671, 1160
- McGaugh, S. S., Schombert, J. M., de Blok, W. J. G., & Zagursky, M. J. 2010, *ApJ*, 708, L14
- Mo, H. J. & White, S. D. M. 1996, *MNRAS*, 282, 347
- Mo, H. J., Yang, X., van den Bosch, F. C., & Jing, Y. P. 2004, *MNRAS*, 349, 205
- Neyrinck, M. C., Szapudi, I., & Szalay, A. S. 2009, *ApJ*, 698, L90
- Pannella, M., Gabasch, A., Goranova, Y., Drory, N., Hopp, U., Noll, S., Saglia, R. P., Strazzullo, V., & et al., 2009, *ApJ*, 701, 787
- Penton, S. V., Stocke, J. T., & Shull, J. M. 2004, *ApJS*, 152, 29
- Press, W. H. & Schechter, P. 1974, *ApJ*, 187, 425
- Reed, D., Gardner, J., Quinn, T., Stadel, J., Fardal, M., Lake, G., & Governato, F. 2003, *MNRAS*, 346, 565
- Reed, D. S., Bower, R., Frenk, C. S., Jenkins, A., & Theuns, T. 2007, *MNRAS*, 374, 2
- Reiprich, T. H. & Böhringer, H. 2002, *ApJ*, 567, 716
- Scodeggio, M., Vergani, D., Cucciati, O., Iovino, A., Franzetti, P., Garilli, B., Lamareille, F., Bolzonella, M., & et al., 2009, *A&A*, 501, 21
- Sheth, R. K. 1998, *MNRAS*, 300, 1057
- Sheth, R. K. & Lemson, G. 1999, *MNRAS*, 305, 946
- Sheth, R. K. & Tormen, G. 1999, *MNRAS*, 308, 119
- . 2002, *MNRAS*, 329, 61
- Springel, V. 2005, *MNRAS*, 364, 1105
- Springel, V., White, S. D. M., Jenkins, A., Frenk, C. S., Yoshida, N., Gao, L., Navarro, J., Thacker, R., & et al., 2005, *Nature*, 435, 629
- Springel, V., White, S. D. M., Tormen, G., & Kauffmann, G. 2001, *MNRAS*, 328, 726
- Sun, M., Voit, G. M., Donahue, M., Jones, C., Forman, W., & Vikhlinin, A. 2009, *ApJ*, 693, 1142
- Tinker, J., Kravtsov, A. V., Klypin, A., Abazajian, K., Warren, M., Yepes, G., Gottlöber, S., & Holz, D. E. 2008, *ApJ*, 688, 709
- Warren, M. S., Abazajian, K., Holz, D. E., & Teodoro, L. 2006, *ApJ*, 646, 881
- Werner, N., Finoguenov, A., Kaastra, J. S., Simionescu, A., Dietrich, J. P., Vink, J., & Böhringer, H. 2008, *A&A*, 482, L29
- York, D. G., Adelman, J., Anderson, Jr., J. E., Anderson, S. F., Annis, J., Bahcall, N. A., Bakken, J. A., Barkhouser, R., & et al. 2000, *AJ*, 120, 1579
- Zentner, A. R. 2007, *International Journal of Modern Physics D*, 16, 763